Wireless Propagation in Circular Tunnels

Donald G. Dudley, *Fellow, IEEE*

***Abstract*—We study models for propagation in circular tunnels. The excitation is either a circular magnetic or circular electric current loop. We produce expressions for the fields in terms of a Fourier transform over the axial variable. We then produce the modes in the lossy structure by contour integration techniques. We include numerical results for the field intensity both as a function of axial distance and as a function of radial distance for several frequencies, radii, and constitutive parameters of interest. We comment in particular concerning the specific form of the field both near to and far from the antenna source.**

***Index Terms*—Cave propagation, lossy circular waveguide, mine communication, tunnel communication, tunnel propagation.**

I. Introduction

In this paper, we consider a model for propagation in lossy circular tunnels. The study has application to communication in highway and railroad tunnels where the cross-sectional geometry is often circular except for the roadbed. In our particular application, the circular tunnel model has relevance to communication in underground nuclear waste storage facilities, such as that planned for Yucca Mountain, Nevada [1]. In such a facility all communication is to be wireless.

Tunnel propagation is not a new subject. Early work focused on applications in the mining industry. Emslie *et al.* [2] considered modes in lossy rectangular tunnels, including propagation around corners, wall roughness, and wall tilt. In [3], Mahmoud and Wait considered models to predict the propagation of both modes and rays in a rectangular tunnel. In one of their models, they assume that the side walls of the tunnel are perfectly conducting, while the top and bottom walls are a lossy dielectric. They produce the rays by the method of stationary phase. They then compare ray and modal results and introduce wall roughness with a simple model that modifies the Fresnel coefficients in the specular direction while neglecting nonspecular contributions. In [4], the same authors consider curved rectangular waveguide with the broad walls imperfectly conducting.

Beginning in the early 1990s, there have appeared a wide variety of papers on tunnel and cave propagation. Mariage, *et al.* [5] applied ray theory and the uniform theory of diffraction (UTD) to propagation in rectangular road tunnels. They also include experimental results. Of particular interest to us is their observation that for axial distances large enough, the field magnitude "decreases nearly exponentially." They further remark that their theoretical results show "beating between higher modes." Nilsson *et al.* [6] used rays to derive an estimate of the ray attenuation in a curved 10×5 m road tunnel. The paper includes experiments by the Norwegian company Telenor. Lienard and Degauque [7] made theoretical calculations for a straight tunnel based on the ray method of Mahmoud and Wait [3]. They observe that "the signal amplitude versus distance between the transmitter and the receiver can be divided into two zones. In the vicinity of the transmitter there are important fluctuations due to the contribution of all higher order modes excited by the transmitting antenna while, at a large distance, the lower order modes become dominant and the attenuation per unit length becomes much smaller." They also included experimental data for more complex mine structures. In two related papers [8], [9], Didascalou, *et al.* introduced a ray tracing method where bundles of rays are used to represent each "physical" wave. Monte Carlo techniques were used for the ray launching. Each bundle of rays was traced to a receiver position where reception spheres determined which rays are intercepted by the receiver. The theory is presented in [8]. Experimental verification, carried out in the Berlin subway system, is provided in [9].

The specific case of the straight circular tunnel can be modeled as a lossy waveguide with circular cross-section. This structure was studied by Wait and Hill [10] to determine the impedance of an elemental electric dipole source. In geophysics, Chew [11], [12] and Lovell and Chew [13] have investigated an elemental dipole source in multilayered cylindrical media, concentrating on the low-frequency case where the modes are so lossy that the primary contribution to the fields is from the continuous spectrum in the form of a lateral wave. Recently, Holloway, *et al.* [14] have considered the homogeneous (source-free) solution in detail. They have numerically evaluated the complex wave number associated with the modes and have produced results for attenuation as a function of frequency on a mode-by-mode basis. In addition, they provide an analytical expression for the field from a small electric dipole. They conclude by commenting on the importance of understanding the propagation channel and remark that "understanding the character of the propagation modes that will be excited by a particular radio system is essential for the design of an effective communication system. They recommend for future work a comprehensive study of the mode excitations produced by various antennas. In this paper, we provide one such study.

We use a circular loop to excite ϕ-symmetric modes. An electric current loop excites TE_z modes, while a magnetic current loop excites those modes TM_z. In both cases we use a Fourier transform $z \leftrightarrow \beta$ and then produce the modes in the lossy structure by contour integration over the poles in the complex β-plane. We develop numerical data and study the field variations both axially and over various cross-sections. We discuss several of the phenomena reported in [5] and [7] and are able to provide analytical reasons for their observations. Finally, we are able to provide insight into strategies for the placing of transmitters and monitoring and communication sensors at various positions in a tunnel. We also provide some criteria for antenna design.

Manuscript received October 25, 2003; revised February 8, 2004.

The author is with the Department of Electrical and Computer Engineering, University of Arizona, Tucson, AZ 85721 USA (e-mail: dudley@dakotacom.net).

Digital Object Identifier 10.1109/TAP.2004.836407

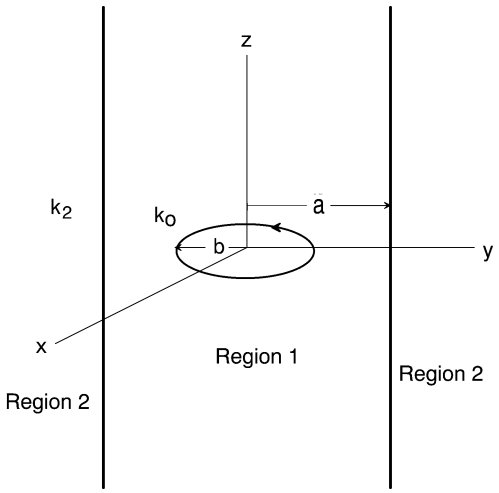

Fig. 1. Circular tunnel.

II. Development of the Model

In what follows, we use $\exp(i\omega t)$ time dependence. Consider a tunnel with circular cross-section (Fig. 1). The structure is excited by a ϕ-independent, axially symmetric circular loop of radius b. The interior $(\rho < a)$ is free space with constitutive parameters (μ_0, ϵ_0). The exterior $(\rho > a)$ is lossy with parameters (μ_0, ϵ), where

$$\epsilon = \epsilon_d + \frac{\sigma}{i\omega}. \tag{1}$$

In (1), ϵ_d is the permittivity of the dielectric with no loss, viz

$$\epsilon_d = \epsilon_0 \epsilon_r \tag{2}$$

and ϵ_r is the dielectric constant. The corresponding wave numbers in the two regions are given by

$$k_0 = \omega\sqrt{\mu_0\epsilon_0}, \quad \rho \in (0, a) \tag{3}$$

$$k_2 = \omega\sqrt{\mu_0\epsilon} = k_0\left(\epsilon_r - i\frac{\sigma}{\omega\epsilon_0}\right)^{1/2}, \quad \rho > a. \tag{4}$$

The current source is either an electric loop J_ϕ with electric dipole moment $I_0 b$, where

$$J_\phi = I_0 b \frac{\delta(\rho - b)}{\rho}\delta(z) \tag{5}$$

or a magnetic loop M_ϕ with magnetic dipole moment $M_0 b$, where

$$M_\phi = M_0 b \frac{\delta(\rho - b)}{\rho}\delta(z). \tag{6}$$

The electric current source excites fields E_ϕ, H_ρ, H_z, whereas the magnetic current source excites H_ϕ, E_ρ, E_z. The former fields are TE_z, while the latter are TM_z. Both sets are ϕ-symmetric. The two cases are independent. We consider them sequentially in what follows.

A. TE_z Case

The solution to the boundary-value problem illustrated in Fig. 1 is a standard exercise in Green's functions. We concentrate on the interval $b < \rho < a$ and obtain, for the electric loop source

$$E_\phi = -\frac{\omega\mu_0 I_0 b}{4}\int_{-\infty}^{\infty} J_1(\lambda b)\left[H_1^{(2)}(\lambda\rho) - \Gamma J_1(\lambda\rho)\right]e^{-i\beta z}\,d\beta \tag{7}$$

$$H_\rho = \frac{1}{i\omega\mu_0}\frac{\partial E_\phi}{\partial z} \tag{8}$$

$$H_z = -\frac{1}{i\omega\mu_0}\left[\frac{1}{\rho}\frac{\partial}{\partial\rho}(\rho E_\phi)\right] \tag{9}$$

where

$$\Gamma = \frac{\lambda H_0^{(2)}(\lambda a)H_1^{(2)}(\lambda_2 a) - \lambda_2 H_0^{(2)}(\lambda_2 a)H_1^{(2)}(\lambda a)}{\lambda J_0(\lambda a)H_1^{(2)}(\lambda_2 a) - \lambda_2 H_0^{(2)}(\lambda_2 a)J_1(\lambda a)} \tag{10}$$

$$\lambda = \left(k_0^2 - \beta^2\right)^{1/2} \tag{11}$$

$$\lambda_2 = \left(k_2^2 - \beta^2\right)^{1/2}. \tag{12}$$

We recognize the first term in the integral in (7) as the $z-\beta$ spectral representation of an electric loop radiating in an unbounded free space medium ([15, pp. 168–171]). The second term is the scattered field produced by the walls. The solution satisfies the following conditions:

1) continuity of the tangential electric and magnetic fields at $\rho = a$;
2) continuity of the Green's function at $\rho = b$;
3) jump condition ([15, p. 62]) at $\rho = b$.
4) appropriate radiation conditions as $\rho \to \infty$ and $z \to \pm\infty$.

We solve the integral by contour integration methods.

We may show that the branch cut in λ, indicated in (11), is not present in the integrand in (7). The proof is omitted. However, the branch cut in λ_2, indicated in (12), survives. In addition, there are poles at $\beta_n a$. We obtain the pole positions at $\beta_n a$ by first finding the λ-plane zeros in the denominator in (10). To find these zeros, we use Müller's method in the Fortran77 IMSL Library. Müller's method requires starting values in the search for the zeros. We use the known zeros for the case with perfectly conducting walls. We display a typical case in Fig. 2 for $f = 1$ GHz, $a = 2$ m, $\sigma = .02$ S/m, $\epsilon_r = 12$. We show the zeros for the perfectly conducting wall case for reference. The transformation to the β-plane is given by

$$\beta_n = \left(k^2 - \lambda_n^2\right)^{1/2} \tag{13}$$

and gives the result in Fig. 3.

To produce an exact result, we must take into account both the pole and branch cut contributions [14]. Because we are interested in the high-frequency fields far from the source, the λ_2 branch cut contribution is negligible [3]. This fact is in direct contrast to the situation in borehole geophysics described by Chew [12], where the borehole diameter is small compared to the wavelength. In such a situation, all of the poles are associated with modes that propagate with great loss. (Such modes are all below cutoff in the case of perfectly conducting walls.) Therefore, in the borehole case, the lateral wave produced by the branch cut is the important contribution. In our case, we de-

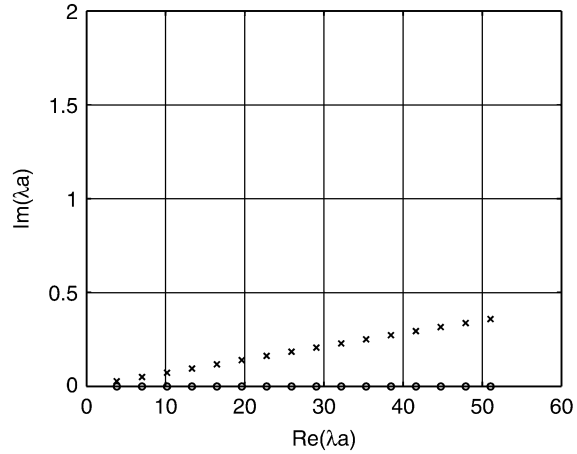

Fig. 2. Poles in the λ-plane, TE$_z$ case; $n = 1, 2, \ldots 16, f = 1$ GHz, $a = 2$ m, $\epsilon_r = 12, \sigma = .02$ S/m. Poles marked with x; poles for perfectly conducting case marked with o.

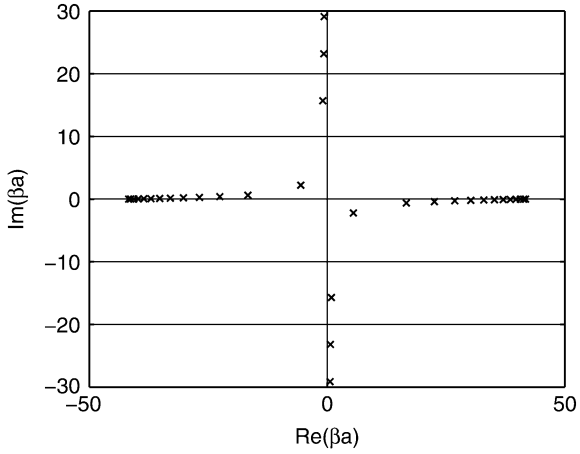

Fig. 3. Poles in the β-plane, TE$_z$ case; $n = 1, 2, \ldots 16, f = 1$ GHz, $a = 2$ m, $\epsilon_r = 12, \sigma = .02$ S/m.

form the integration contour in (7) to capture the poles in the fourth quadrant of the β-plane. This procedure gives the fields, for $z > 0, b < \rho < a$, in terms of the pole residues, viz

$$E_{\phi 1} = -\frac{\pi i \omega \mu_0 I_0 b}{2a} \sum_{n=1}^{\infty} J_1(\lambda_n b) J_1(\lambda_n \rho) e^{-i\beta_n z} \frac{N_n}{D_n} \quad (14)$$

where

$$\begin{aligned} N_n &= \lambda_n a H_0^{(2)}(\lambda_n a) H_1^{(2)}(\lambda_{2,n} a) \\ &\quad - \lambda_{2,n} a H_0^{(2)}(\lambda_{2,n} a) H_1^{(2)}(\lambda_n a) \quad (15) \\ D_n &= \lim_{\beta \to \beta_n} \frac{d}{d\beta} \left[\lambda J_0(\lambda a) H_1^{(2)}(\lambda_2 a) \right. \\ &\quad \left. - \lambda_2 H_0^{(2)}(\lambda_2 a) J_1(\lambda a) \right] \\ &= \beta_n a \left[\left(\frac{\lambda_n}{\lambda_{2,n}} \frac{1}{\lambda_{2,n} a} - \frac{1}{\lambda_n a} \right) J_0(\lambda_n a) H_1^{(2)}(\lambda_{2,n} a) \right. \\ &\quad + \left(\frac{\lambda_{2,n}}{\lambda_n} - \frac{\lambda_n}{\lambda_{2,n}} \right) J_0(\lambda_n a) H_0^{(2)}(\lambda_{2,n} a) \\ &\quad \left. + \left(\frac{1}{\lambda_{2,n} a} - \frac{\lambda_{2,n}}{\lambda_n} \frac{1}{\lambda_n a} \right) J_1(\lambda_n a) H_0^{(2)}(\lambda_{2,n} a) \right]. \quad (16) \end{aligned}$$

B. TM$_z$ Case

The TM$_z$ case proceeds along similar lines. Using the magnetic current loop given in (6), we obtain

$$\begin{aligned} H_\phi &= -\frac{\omega \epsilon_0 M_0 b}{4} \int_{-\infty}^{\infty} \left[H_1^{(2)}(\lambda \rho) - \hat{\Gamma} J_1(\lambda \rho) \right] \\ &\quad \cdot J_1(\lambda b) e^{-i\beta z} \, d\beta, \quad b < \rho < a \quad (17) \\ E_\rho &= -\frac{1}{i\omega\epsilon_0} \frac{\partial H_\phi}{\partial z} \quad (18) \\ E_z &= -\frac{1}{i\omega\epsilon_0} \left[\frac{1}{\rho} \frac{\partial}{\partial \rho} (\rho H_\phi) \right] \quad (19) \end{aligned}$$

where

$$\hat{\Gamma} = \frac{\kappa \lambda H_0^{(2)}(\lambda a) H_1^{(2)}(\lambda_2 a) - \lambda_2 H_0^{(2)}(\lambda_2 a) H_1^{(2)}(\lambda a)}{\kappa \lambda J_0(\lambda a) H_1^{(2)}(\lambda_2 a) - \lambda_2 H_0^{(2)}(\lambda_2 a) J_1(\lambda a)} \quad (20)$$

and where κ is the complex dielectric constant, given by

$$\kappa = \epsilon_r + \frac{\sigma}{i\omega\epsilon_0}. \quad (21)$$

We find again that the branch cut in λ is annihilated. However, the branch cut in λ_2 survives. Again, we are interested in the fields far from the source where the λ_2 branch cut contribution is negligible [3]. We therefore find the fields in terms of the residues only, viz

$$H_{\phi 1} = -\frac{\pi i \omega \epsilon_0 M_0 b}{2a} \sum_{n=1}^{\infty} J_1(\lambda_n b) J_1(\lambda_n \rho) e^{-i\beta_n z} \frac{\hat{N}_n}{\hat{D}_n} \quad (22)$$

where

$$\begin{aligned} N_n &= \kappa \lambda_n a H_0^{(2)}(\lambda_n a) H_1^{(2)}(\lambda_{2,n} a) \\ &\quad - \lambda_{2,n} a H_0^{(2)}(\lambda_{2,n} a) H_1^{(2)}(\lambda_n a) \quad (23) \\ D_n &= \lim_{\beta \to \beta_n} \frac{d}{d\beta} \left[\kappa \lambda J_0(\lambda a) H_1^{(2)}(\lambda_2 a) - \lambda_2 H_0^{(2)}(\lambda_2 a) J_1(\lambda a) \right] \\ &= \beta_n a \left[\kappa \left(\frac{\lambda_n}{\lambda_{2,n}} \frac{1}{\lambda_{2,n} a} - \frac{1}{\lambda_n a} \right) J_0(\lambda_n a) H_1^{(2)}(\lambda_{2,n} a) \right. \\ &\quad + (\kappa - 1) J_1(\lambda_n a) H_1^{(2)}(\lambda_{2,n} a) \\ &\quad + \left(\frac{\lambda_{2,n}}{\lambda_n} - \frac{\kappa \lambda_n}{\lambda_{2,n}} \right) J_0(\lambda_n a) H_0^{(2)}(\lambda_{2,n} a) \\ &\quad \left. + \left(\frac{1}{\lambda_{2,n} a} - \frac{\lambda_{2,n}}{\lambda_n} \frac{1}{\lambda_n a} \right) J_1(\lambda_n a) H_0^{(2)}(\lambda_{2,n} a) \right]. \quad (24) \end{aligned}$$

III. Numerical Results

We give results for both the TE$_z$ and TM$_z$ cases and follow with a discussion.

A. TE$_z$ Case

We initially consider the following parameters:

- $f = 1$ GHz;
- $a = 2$ m;
- $\sigma = .02$ S/m;
- $\epsilon_r = 12$;
- $\rho/a = .3$;
- $b/a = .05$.

To determine the number of modes required for convergence, we examine the number of modes above cutoff for perfectly

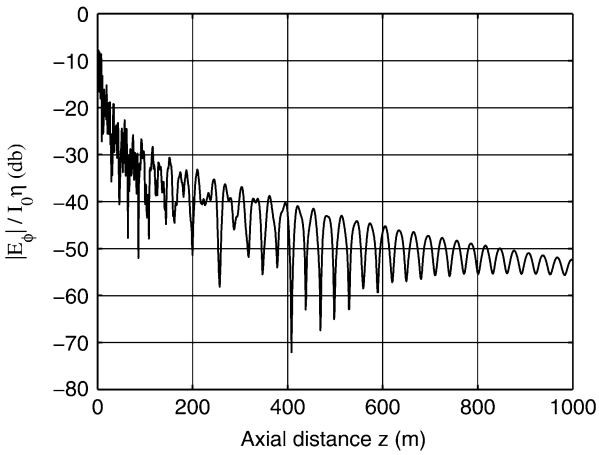

Fig. 4. E-field (decibels) versus axial distance $z \in (0, 1000)$ m, TE_z case; $n = 1, 2, \ldots 16, f = 1$ GHz, $a = 2$ m, $\epsilon_r = 12, \sigma = .02$ S/m, $\rho/a = .3, b/a = .05$.

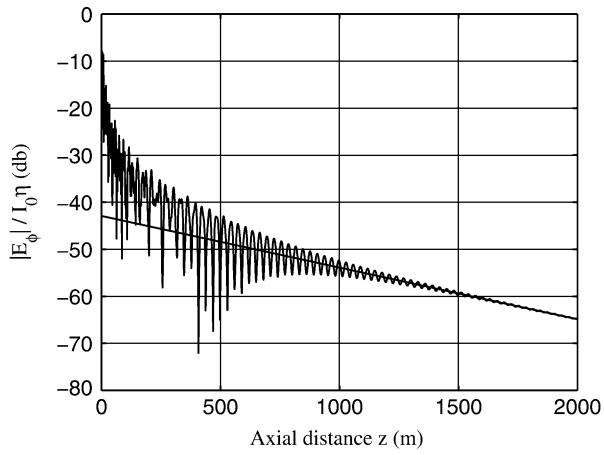

Fig. 5. E-field (decibels) versus axial distance $z \in (0, 2000)$ m, TE_z case; $n = 1, 2, \ldots 16, f = 1$ GHz, $a = 2$ m, $\epsilon_r = 12, \sigma = .02$ S/m, $\rho/a = .3, b/a = .05$; straight line is the field for the $n = 1$ mode only.

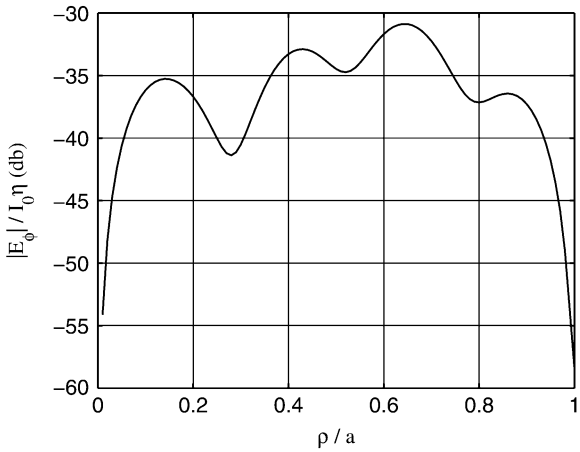

Fig. 6. E-field (decibels) versus normalized radial distance ρ/a at $z = 100$ m, TE_z case; $n = 1, 2, \ldots 16, f = 1$ GHz, $a = 2$ m, $\epsilon_r = 12, \sigma = .02$ S/m, $\rho/a = .3, b/a = .05$.

conducting walls. The cutoff condition for the TE_{0m} modes is given by

$$f_m^{(c)} = \frac{c}{2\pi a} p_{0m} \tag{25}$$

where $f_m^{(c)}$ is the cutoff frequency of the mth mode, c is the speed of light and p_{0m} is the mth root of the first-order Bessel function, viz

$$J_1(x) = 0. \tag{26}$$

We solve for p_{0m} in (25) with $f = 1$ GHz and $a = 2$ m and obtain the condition for the modes to be evanescent, as follows:

$$p_{0m} > 41.9. \tag{27}$$

We use the asymptotic form for $J_1(x)$ ([16, p. 462]) and find the asymptotic roots from

$$\cos\left(x - \frac{3\pi}{4}\right) = 0. \tag{28}$$

The result for the listed parameters is that 13 modes are above cutoff for perfectly conducting walls. We use 16 modes to assure convergence in the lossy wall case.

We display the results in Fig. 4. The plot shows the two-zone feature discussed by Lienard and Degauque [7]. For a zone given by $z < 400$ m, there are rapid variations in the field over small distances. These variations are caused by the mutual interference among many modes traveling at different phase velocities. For a zone given by $z > 400$ m, the variations with axial distance become smoother. Indeed, we find that if we sum only the $n = 1$ and $n = 2$ modes, we produce a plot that, for $z > 550$ m, is the same as that in Fig. 4, within the accuracy of the plot.

In [5], Mariage *et al.* indicate that, for axial distances large enough, the field magnitude "decreases nearly exponentially." We verify this statement analytically by considering the field produced by only the $n = 1$ mode, viz

$$E_{\phi 1}^{(1)} = A(\rho) e^{-i\beta_1 z} \tag{29}$$

where $\mathrm{Im}(\beta_1) < 0$. In decibels

$$dB(|E_{\phi 1}|) = 20 \log_{10} |A| + 8.686[\mathrm{Im}(\beta_1)]z. \tag{30}$$

In Fig. 5, we show that the field relaxes to the field produced by the $n = 1$ mode for z large enough. This field is exponential, or linear in decibels, with a slope of $8.686[\mathrm{Im}(\beta_1)]$. In this case, the fall-off is approximately 10 dB per 1000 m. This should be compared with the initial fall-off of approximately 40 dB in the initial 1000 m.

The local variations are particularly rapid in the interval from zero to 400 m and are as high as 30 dB in amplitude. This result shows that the placement of receivers in a tunnel can produce signals that vary dramatically with small changes in axial location.

We also examine the variations over the cross-section at an axial distance of 100 m (Fig. 6). Since the ϕ-directed field is tangential to the wall, the field falls off rapidly near $\rho/a = 1$. In addition, by symmetry, the field is zero at $\rho = 0$.

We repeat the presentation with the same parameters as listed above, except we change the frequency to $f = 2$ GHz. In this case, we find that there are 26 modes above cutoff for perfectly conducting walls. We use 29 modes to assure convergence. Searching for 29 roots produces instabilities in Müller's method. We solve this difficulty by requiring Müller's method to search for the first 14 roots and then rerunning the algorithm to search for the next 15. Using this bisection results in a maximum of eight iterations in the search for any root.

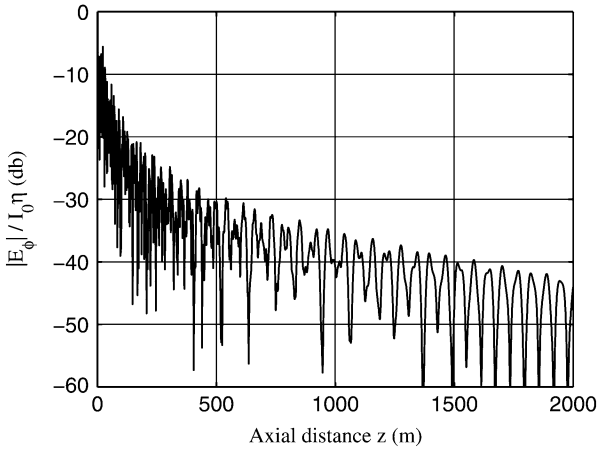

Fig. 7. E-field (decibels) versus axial distance z, TE_z case; $n = 1, 2, \ldots 29$, $f = 2$ GHz, $a = 2$ m, $\epsilon_r = 12, \sigma = .02$ S/m, $\rho/a = .3, b/a = .05$.

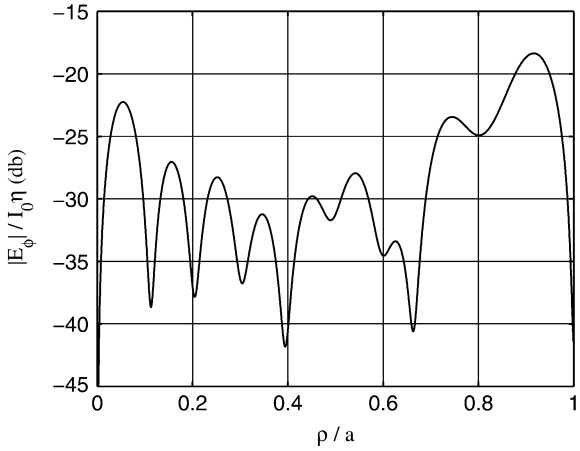

Fig. 8. E-field (decibels) versus normalized radial distance ρ/a at $z = 100$ m, TE_z case; $n = 1, 2, \ldots 29, f = 2$ GHz, $a = 2$ m, $\epsilon_r = 12, \sigma = .02$ S/m, $\rho/a = .3, b/a = .05$.

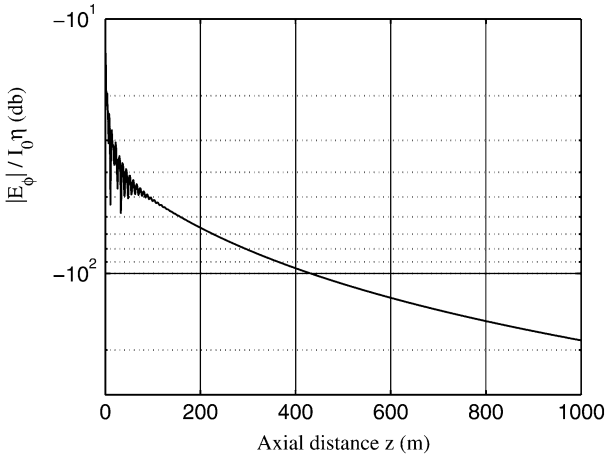

Fig. 9. E-field (decibels) versus axial distance z, TE_z case; $n = 1, 2, \ldots 10$, $f = 1$ GHz, $a = 1$ m, $\epsilon_r = 5, \sigma = .02$ S/m, $\rho/a = .3, b/a = .05$. (Note: Vertical axis is log scale.)

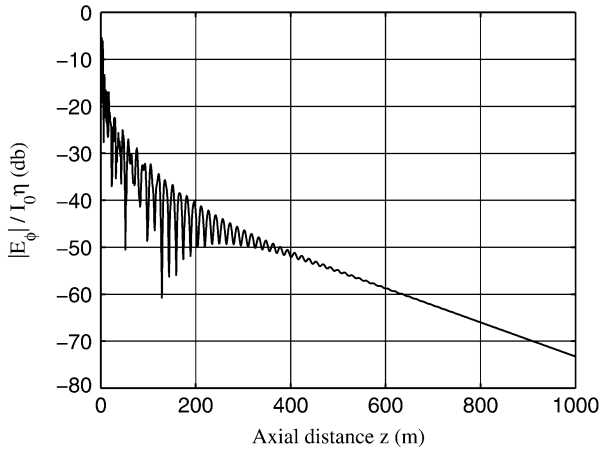

Fig. 10. E-field (decibels) versus axial distance z, TE_z case; $n = 1, 2, \ldots 16$, $f = 2$ GHz, $a = 1$ m, $\epsilon_r = 5, \sigma = .02$ S/m, $\rho/a = .3, b/a = .05$.

We display results for the field strength versus axial distance in Fig. 7. Whereas the trend in the field strength indicated a fall-off of 40 dB in 1000 m at $f = 1$ GHz, at 2 GHz the fall-off is approximately 25 dB. We have plotted the result over 2000 m to demonstrate that, at the higher frequency, the higher order modal interference is significant at a longer distance than in the 1 GHz case.

We next examine the variations over a cross-section at $z = 100$ m (Fig. 8). We note an increase in the number of oscillations. In addition the field strength varies locally by as much as 15 dB at some cross-sectional positions.

We next consider the case of a smaller tunnel with the following parameters:

- $a = 1$ m;
- $\sigma = .02$ S/m;
- $\epsilon_r = 5$;
- $\rho/a = .3$;
- $b/a = .05$.

We note that the tunnel cross-section has been reduced by a factor of 2 and the dielectric constant has been reduced to 5. In Figs. 9–12, we display results for the field intensity versus axial distance for $f = 1, 2, 3, 4$ GHz, respectively. At $f = 1$ GHz (Fig. 9), there are six modes above cutoff for perfectly conducting walls. We use 10 modes in our data. In 1000 m, the field intensity decreases approximately 160 dB. This rapid fall-off indicates that the frequency is too low for effective tunnel propagation. At 2 GHz (Fig. 10), there are 13 modes above cutoff. We use 16 modes in our data. The fall-off at 1000 m is approximately 55 dB. In addition, there are local oscillations as much as 20 dB in extent out to distances of about 300 m. At 3 GHz (Fig. 11), there are 19 modes above cutoff. We use 23 modes in our data. The fall-off is approximately 42 dB in 1000 m. Finally, at 4 GHz (Fig. 12), there are 26 modes above cutoff. We use 29 modes in our analysis. The fall-off at 1000 m is approximately 35 dB. We summarize this data in Table I. Finally, in this case with reduced cross-section, we note the same richness of modal content at distances near to the source. Again, the lower order modes dominate at larger distances.

B. TM_z Case

We first consider the same parameters as initially examined in the TE_z case, viz:

- $f = 1$ GHz;
- $a = 2$ m;
- $\sigma = .02$ S/m;

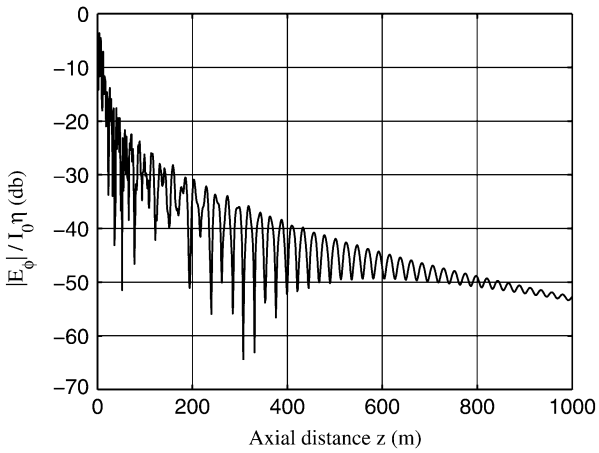

Fig. 11. E-field (decibels) versus axial distance z, TE_z case; $n = 1, 2, \ldots 23$, $f = 3$ GHz, $a = 1$ m, $\epsilon_r = 5, \sigma = .02$ S/m, $\rho/a = .3, b/a = .05$.

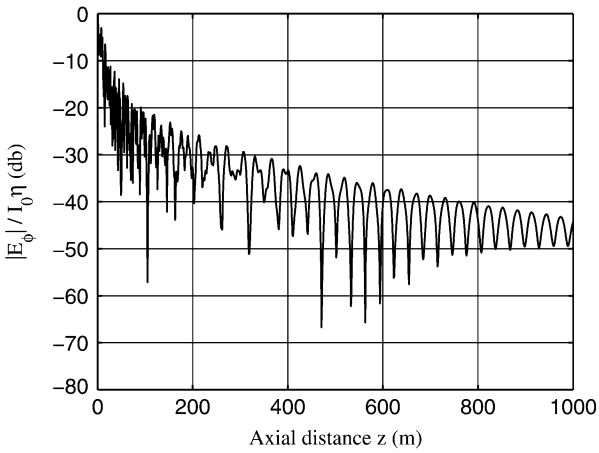

Fig. 12. E-field (decibels) versus axial distance z, TE_z case; $n = 1, 2, \ldots 29$, $f = 4$ GHz, $a = 1$ m, $\epsilon_r = 5, \sigma = .02$ S/m, $\rho/a = .3, b/a = .05$.

TABLE I
FALL-OFF OF FIELD INTENSITY (DECIBELS) IN 1000 m, TE_z CASE; $a = 1$ m, $\sigma = .02$ S/m, $\epsilon_r = 5, \rho/a = .3, b/a = .05$

f (GHz)	# of modes	figure #	db in 1 km
1	10	9	150
2	16	10	55
3	23	11	42
4	29	12	35

- $\epsilon_r = 12$;
- $\rho/a = .3$;
- $b/a = .05$.

To determine the number of modes required for convergence, we once more examine the number of modes above cutoff for perfectly conducting walls. The cutoff condition for the TM_{0m} modes is given by

$$f_m^{(c)} = \frac{c}{2\pi a} q_{0m} \tag{31}$$

where $f_m^{(c)}$ is the cutoff frequency of the mth mode, c is the speed of light and q_{0m} is the mth root of the zeroth order Bessel function, viz

$$J_0(x) = 0. \tag{32}$$

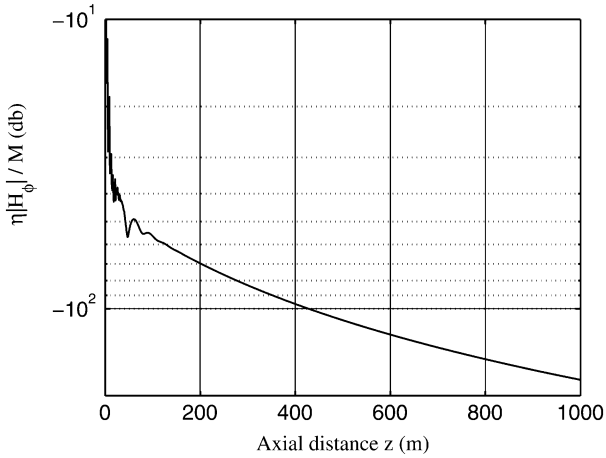

Fig. 13. H-field (decibels) versus axial distance z, TM_z case; $n = 1, 2, \ldots 16$, $f = 1$ GHz, $a = 2$ m, $\epsilon_r = 12, \sigma = .02$ S/m, $\rho/a = .3, b/a = .05$. (Note: Vertical axis is log scale.).

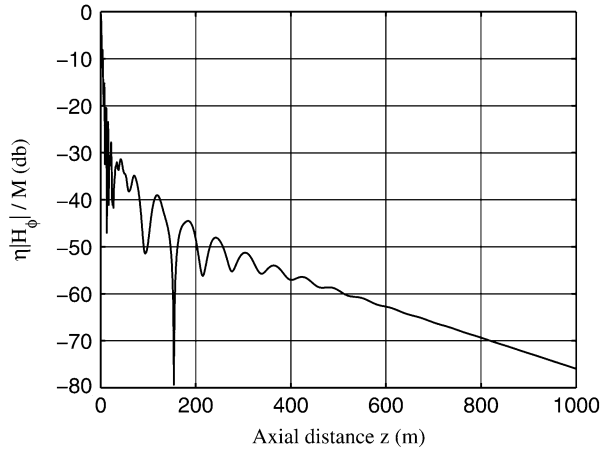

Fig. 14. H-field (decibels) versus axial distance z, TM_z case; $n = 1, 2, \ldots 29$, $f = 2$ GHz, $a = 2$ m, $\epsilon_r = 12, \sigma = .02$ S/m, $\rho/a = .3, b/a = .05$.

We solve for q_{0m} in (25) with $f = 1$ GHz and $a = 2$ m and obtain the same condition for the TM_z modes to be evanescent, as follows:

$$q_{0m} > 41.9. \tag{33}$$

We use the asymptotic form for $J_0(x)$ ([16p. 462]) and find the asymptotic roots from

$$\cos\left(x - \frac{\pi}{4}\right) = 0. \tag{34}$$

The result for the listed parameters is that, identical to the TE_z case, there are 13 modes above cutoff for perfectly conducting walls. We use 16 modes to assure convergence for the lossy walls.

We show the result for 1 GHz in Fig. 13 and for 2 GHz in Fig. 14. For 1 GHz, the fall-off in the field is approximately 170 dB in 1000 m. For 2 GHz, we use 29 modes and find that the fall-off is approximately 60 dB. In comparison with the same parameters in the TE_z case (Figs. 4 and 7), it is clear that the fall-off is much more severe for the magnetic current excitation, 170 versus 40 dB at 1 GHz and 60 versus 25 dB at 2 GHz. The severity of the attenuation leads us to omit further consideration of the TM_z modes for the smaller tunnel.

IV. Discussion

It is clear that the electric current loop exciting the TE_z modes is preferable over the magnetic current loop exciting the TM_z modes. This result is consistent with the fact that in the TE_z case, the electric field is totally tangential to the wall. If the wall were perfectly conducting, the tangential field vanishes at the wall. In our lossy case it is still quite small. This situation is described in basic texts ([17, pp. 485–489]) where it is shown that the TE_{01} mode has much lower attenuation characteristics than any other mode. For circular tunnels, such considerations point to the use of an electric current loop or a helix ([18, pp. 301–307]), in circularly polarized mode, as an exciting antenna. This antenna should be located in the center of the tunnel cross-section where it couples strongly to the TE_{01} mode.

The principal limitation to our analysis is that our source produces only TE_{0m} or TM_{0m} modes. However, a linearly polarized current source [14] is clearly an option for tunnel propagation. Such a source excites hybrid modes. For the circular tunnel, described herein, we postulate that the ϕ-symmetric circular electric loop source, described herein, is optimum, in the sense that it gives the minimum path loss at long axial distances in a straight tunnel. To verify this postulate, we plan to examine the axial propagation characteristics in the linear source problem as a next step in understanding circular tunnel propagation. The formulation has been described in [10], [14] and, for the multicylindrically layered medium, in [13], ([11, pp. 161–184]). It remains to do the numerical reduction and thereby answer the question concerning how much worse the axial attenuation becomes in the cases without ϕ-symmetry. Our "optimum" postulate indicates that, at this juncture, we do not believe that we can improve on the path loss figures in our TE_z results herein.

Finally, we emphasize again the rapid local variations in the field as a function of axial distance. This result is not confined to cases with ϕ-symmetry. Indeed, other authors considering other geometries display similar features [5]–[7], [9]. We remark that the rapid variation does not appear in the results reported in [3], for the rectangular case of two perfectly conducting walls and two lossy walls. We have found that, although their result is correct for the points plotted, the coarse nature of their data digitization produces their smoother result. We have reformulated their problem, reproduced their result, incorporated a finer digitization, and found rapid variations similar to those discussed herein.

Acknowledgment

This work was accomplished under a consulting agreement with Lawrence Livermore National Laboratory. The author thanks H.-Y. Pao for his support and K. F. Casey for many stimulating and helpful discussions. The author also thanks the reviewers, whose comments have led to a substantial revision of the original submission.

References

[1] U.S. Department of Energy. (2002, Feb.) Yucca Mountain Science and Engineering Report, Rev. 1. [Online]. Available: www.ocrwm.doe.gov/documents/ser-b/toc.htm

[2] A. G. Emslie, R. L. Lagace, and P. F. Strong, "Theory of the propagation of uhf radio waves in coal mine tunnels," *IEEE Trans. Antennas Propagat.*, vol. AP-23, pp. 192–205, 1975.

[3] S. F. Mahmoud and J. R. Wait, "Geometrical optical approach for electromagnetic wave propagation in rectangular mine tunnels," *Radio Sci.*, vol. 9, pp. 1147–1158, 1974.

[4] ——, "Guided electromagnetic waves in a curved rectangular mine tunnel," *Radio Sci.*, vol. 9, pp. 567–572, 1974.

[5] P. Mariage, M. Lienard, and P. Degauque, "Theoretical and experimental approach of the propagation of high frequency waves in road tunnels," *IEEE Trans. Antennas Propagat.*, vol. 42, pp. 75–81, 1994.

[6] M. Nilsson, J. Slettenmark, and C. Beckman, "Wave propagation in a curved tunnel," in *Proc. IEEE AP-S Int. Symp. Dig.*, 1998, pp. 1876–1879.

[7] M. Lienard and P. Degauque, "Natural wave propagation in mine environments," *IEEE Trans. Antennas Propagat.*, vol. 48, pp. 1326–1339, 2000.

[8] D. Didascalou, T. M. Schafer, F. Weinmann, and W. Wiesbeck, "Ray-density normalization for ray-optical wave propagation modeling in arbitrarily shaped tunnels," *IEEE Trans. Antennas Propagat.*, vol. 48, pp. 1316–1325, 2000.

[9] D. Didascalou, J. Maurer, and W. Wiesbeck, "Subway tunnel guided electromagnetic wave propagation at mobile communications frequencies," *IEEE Trans. Antennas Propagat.*, vol. 49, pp. 1590–1595, 2001.

[10] J. R. Wait and D. A. Hill, "Impedance of an electric dipole located in a cylindrical cavity in a dissipative medium," *Appl. Phys.*, vol. 11, pp. 351–356, 1976.

[11] W. C. Chew, *Waves and Fields in Inhomogeneous Media*. New York: IEEE Press, 1995.

[12] ——, "Response of a current loop antenna in an invaded borehole," *Geophys.*, vol. 49, pp. 81–91, 1984.

[13] J. R. Lovell and W. C. Chew, "Response of a pont source in a multicylindrically layered medium," *IEEE Trans. Geoscience Remote Sensing*, vol. GE-25, pp. 850–858, 1987.

[14] C. L. Holloway, D. A. Hill, R. A. Dalke, and G. A. Hufford, "Radio wave propagation characteristics in lossy circular waveguides such as tunnels, mine shafts, and boreholes," *IEEE Trans. Antennas Propagat.*, vol. 48, pp. 1354–1365, 2000.

[15] D. G. Dudley, *Mathematical Foundations for Electromagnetic Theory*. New York: IEEE Press, 1994.

[16] R. F. Harrington, *Time-Harmonic Electromagnetic Fields*. New York: IEEE Press, 2001.

[17] C. A. Balanis, *Advanced Engineering Electromagnetics*. New York: Wiley, 1989.

[18] J. D. Kraus, *Antennas*, 2nd ed. New York: McGraw-Hill, 1988.

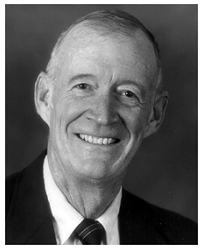

Donald G. Dudley (M'83–SM'87–F'90) received the B.S. degree from Virginia Polytechnic Institute and State University, Blacksburg, and the M.S. and Ph.D. degrees from the University of California, Los Angeles.

At the University of Arizona, Tucson, he is one of the founding members of the Program in Applied Mathematics. He founded the Electromagnetics Laboratory in the Department of Electrical and Computer Engineering and served eight years as its Director. He has twice been elected by students in the College of Engineering and Mines as the Outstanding Professor of the Year. Currently, he is Professor Emeritus in the Department of Electrical and Computer Engineering, University of Arizona, and a Consultant in electromagnetics. He is the author of over 70 papers and 200 abstracts in electromagnetics, plus the book *Mathematical Foundations for Electromagnetic Theory* (New York: IEEE Press, 1994). He is the Series Editor of the *IEEE Press Series on Electromagnetic Wave Theory* (22 titles). He has served as an Associate Editor of the journal *Radio Science*. His principal research interests are in the mathematical foundations of electromagnetics, electromagnetic system identification, integral equations, and inverse theory

Professor Dudley is a Member of Commissions B and F of the International Union of Radio Science (URSI). He has served as Chairman of the U.S. Commission on Fields and Waves (Commission B) and as a Member of the U.S. National Committee (USNC). In 1997, he was the co-recipient of the Schelkunoff Prize for Best Paper of the Year in the IEEE Transactions on Antennas and Propagation. In 2000, he was awarded an IEEE Third Millennium Medal. In 2002, he was presented with the Chen-To Tai Distinguished Educator Award by the IEEE Antennas and Propagation Society. He has served as a Member of the Administrative Committee of the IEEE Antennas and Propagation Society (APS), as an Associate Editor of the IEEE Transactions on Antennas and Propagation, as Chairman of the IEEE Electromagnetics Field Award Committee, and as a Member of the IEEE/APS Education Committee.